analytical chemistry

pubs.acs.org/ac Article

Accelerating Restricted Diffusion NMR Studies with Time-Resolved and Ultrafast Methods

Mateusz Urbańczyk, Yashu Kharbanda, Otto Mankinen, and Ville-Veikko Telkki*

Cite This: *Anal. Chem.* 2020, 92, 9948−9955 Read Online

ACCESS | Metrics & More | Article Recommendations

ABSTRACT: Restricted diffusion of fluids in porous materials can be studied by pulsed field gradient nuclear magnetic resonance (NMR) non-invasively and without tracers. If the experiment is repeated many times with varying diffusion delays, detailed information about pore sizes and tortuosity can be recorded. However, the measurements are very time-consuming because numerous repetitions are needed for gradient ramping and varying diffusion delays. In this paper, we demonstrate two different strategies for acceleration of the restricted diffusion NMR measurements: time-resolved diffusion NMR and ultrafast Laplace NMR. The former is based on time-resolved non-uniform sampling, while the latter relies on spatial encoding of two-dimensional data. Both techniques allow similar 1−2 order of magnitude acceleration of acquisition, but they have different strengths and weaknesses, which we discuss in detail. The feasibility of the methods was proven by investigating restricted diffusion of water inside tracheid cells of thermally modified pine wood.

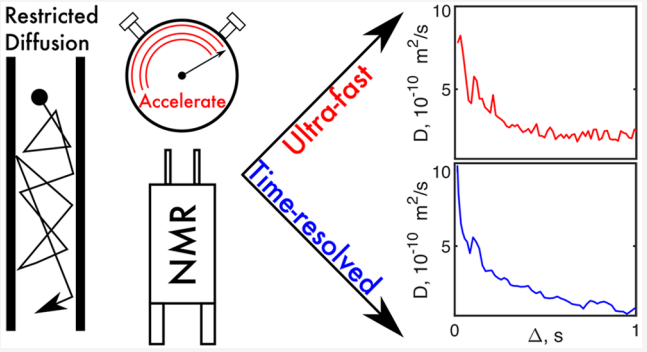

Nuclear magnetic resonance (NMR) diffusion experiments have been widely exploited in the studies of structures and fluid transport properties of porous materials.[1] The applications of the method include rocks,[2] glass beads,[3] wood,[4,5] ionic liquids,[6,7] cells,[8,9] sol−gel-made silica particles,[10] polymers,[11] aerogels,[12] zeolites,[13] metal organic frameworks,[14] etc. The walls of pores restrict the diffusion of absorbed fluid molecules. Repeating the NMR diffusion experiment many times with an increasing diffusion time (Δ) will make this effect visible.[2,3] The longer the Δ, the more restricted the diffusion and therefore the smaller the observed apparent diffusion coefficient. Unfortunately, the restricted diffusion measurements are time-consuming because the experiment has to be repeated multiple times with varying diffusion gradient strengths (g_D) and times (Δ).

In the conventional two-dimensional NMR experiment (like the diffusion NMR experiment), one has to repeat the pulse sequence for each indirect point, leading to a very long experiment time. This problem was circumvented by spatial encoding of the indirect dimension in the method called ultrafast NMR (UF NMR).[15−17] The difference between the acquisition strategies of the conventional and UF experiments is illustrated in Figure 1. The method allowed one to acquire two-dimensional data in a single scan. The single-scan approach also reveals the possibility of utilizing hyperpolarization techniques to boost the sensitivity of the experiment by several orders of magnitude.[18,19] The method was also adapted successfully to the Laplace NMR,[20] comprising relaxation and diffusion experiments, allowing single-scan measurements of conventional diffusion ordered spectroscopy (DOSY),[21−25] or even two-dimensional (2D) Laplace correlation maps like T_1-T_2[26−28] and $D-T_2$,[28−30] as well as diffusion exchange spectroscopy (DEXSY).[31]

Another strategy developed for accelerating multidimensional NMR investigations of time-dependent processes is time-resolved non-uniform sampling (TR-NUS), first proposed by Mayzel et al.[32] The method was initially used to study the kinetics of in vitro phosphorylation of protein. The idea is based on the NUS acquisition of the spectra with a long oversampled NUS scheme of indirect dimensions and later dividing the data into overlapping subsets (frames) and reconstructing them. The resulting set of spectra allows for a good temporal resolution as each subset highly overlaps with previous spectra in the reaction time dimension. The concept was successfully used in other reaction studies[33−36] and also extended to the studies in which one analyzes the dependence of the parameter on temperature[37] or INEPT transfer time.[38] The idea was also adapted for diffusion-based reaction

Received: April 9, 2020
Accepted: June 18, 2020
Published: June 18, 2020

https://dx.doi.org/10.1021/acs.analchem.0c01523
Anal. Chem. 2020, 92, 9948−9955

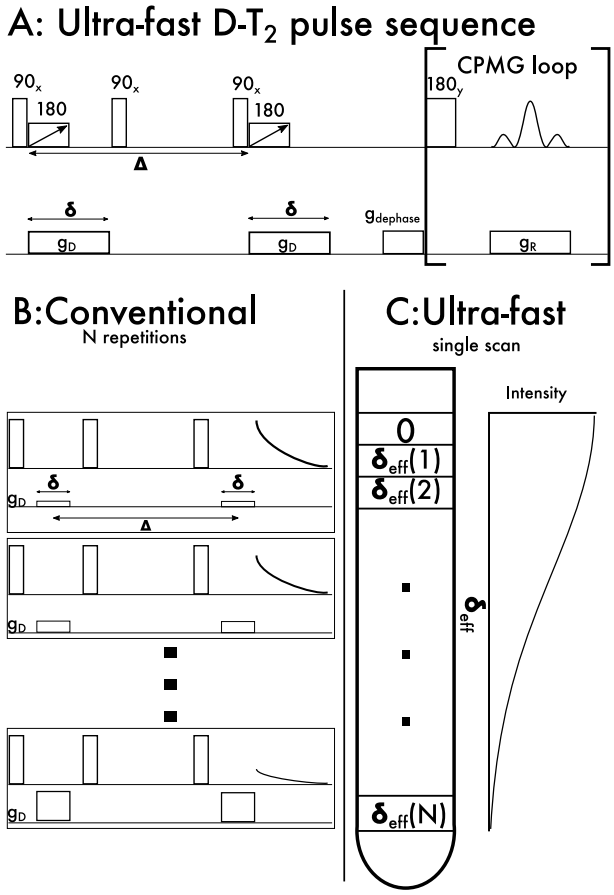

Figure 1. Difference between diffusion NMR acquisition strategies in the UF and conventional experiments. (A) UF $D-T_2$ pulse sequence used in this study. (B) Conventional PGSTE acquisition scheme. The acquisition is repeated many times by varying the strengths of gradient pulses. (C) In the UF $D-T_2$ experiment, corresponding diffusion data are encoded into the layers of the sample, as the frequency-swept 180° pulse makes the effective length of the gradient pulse linearly dependent on position.

monitoring[39,40] utilizing the concept of permuted DOSY (p-DOSY).[41] As for TR-NUS, TR diffusion NMR can also be exploited in the analysis of the parameter space instead of the temporal space. The idea of TR diffusion NMR is illustrated in Figure 2.

In this paper, we demonstrate that the restricted diffusion measurements can be significantly accelerated by the UF and TR methods. We study the diffusion of water molecules inside tracheid cells of thermally modified pine wood samples as a function of diffusion time Δ. We compare the results obtained by the two methods and cross-check them with the literature values. We also analyze the strengths and weaknesses of the methods.

EXPERIMENTAL SECTION

Sample Preparation. A pine wood (*Pinus sylvestris*) plank was dried at 70 °C. After that, the plank was thermally modified at 200 °C using the Thermowood process.[42] After the process, a cylindrical sample (axis along the radial direction) with a diameter of 3 mm was cut and submerged in distilled water for 2 weeks to saturate the cells with the solvent. Before the acquisition, the sample was transferred to a 10 mm NMR tube and fixed with Teflon tape to prevent it from moving due to shaking caused by gradients.

NMR Measurements. NMR experiments were performed on a Bruker Avance III 300 MHz spectrometer equipped with a micro 2.5 microimaging unit, using a 10 mm RF insert.

UF $D-T_2$. The ultrafast $D-T_2$ pulse sequence was set with a δ of 7 ms and Δ values of 15−1004 ms (total of 67 experiments). Because of the linear dependence of the Stejskal−Tanner equation[43] on Δ, the strength of the diffusion gradient has to be adapted when Δ is changed to have reasonable signal amplitudes. The g_D was decreased after each Δ step below 100 ms. At higher Δ values, the value was changed only every 100 ms of Δ range. To keep the spatial encoding height range constant, the sweep width of the frequency-swept chirp refocusing pulse was decreased along with its power. Therefore, the experiments required altogether 15 different chirp pulses. The length of the hard $\pi/2$ pulse was 16.25 μs. The number of echoes was 64, the echo time 9.5 ms, and the number of scans 16 with a repetition time of 3 s. Each echo was acquired with 256 complex points. The experiment time of a single experiment was only ∼1 min, and the total time required to record the whole Δ dependence of the diffusion coefficient was 78 min.

The acquisition was followed by the Fourier transform in the spatial frequency dimension and removal of the data outside the spatial encoding region. The resulting data (analogous to the conventional $D-T_2$ correlation experiment) matrix was 150 × 64 points. The excitation−detection sensitivity profile of the coil influences the detected spatially encoded data along the *z*-direction. To abolish this effect, we performed one-dimensional MRI of the sample along the *z*-axis with the same imaging parameters as in the CPMG loop of the ultrafast $D-T_2$ experiment. The acquired coil excitation−detection profile was used to eliminate the effect of the sensitivity profile. After that, the *z*-axis was converted into the spatial frequency δ-axis by using a linear relationship between them.

The $D-T_2$ maps were obtained by a 2D Laplace inversion using 2D ITAMeD implementation.[44−46] The apparent diffusion coefficients as a function of Δ were extracted from biexponential fits with the diffusion decay profiles corresponding to the first echo. The faster diffusion coefficient was interpreted to represent the diffusion of free water inside lumens of tracheid cells.

TR Diffusion NMR. The TR diffusion NMR experiment was measured using 66 semirandom pulsed field gradient strengths. A set of linearly increasing gradient strength values (in this case 16 values) was randomly permuted, and then this permuted gradient strength value scheme was repeated to cover the long sampling space. During the sampling, Δ was linearly increased and the length of the gradient pulse, δ, was decreased to keep the signal intensity stable. In the first 10 measurement steps, a constant Δ value of 15 ms was used to ensure that the first frame provides information about the shortest diffusion time. Thereafter, the Δ value was changed linearly from 15 to 1000 ms. The δ parameter was decreased proportionally to $\Delta^{-1/2}$ from 4 to 0.5 ms. The standard Bruker stimulated echo diffusion pulse sequence stegp1s1d was used in the experiments, and the acquisition queue was created using a modified TReNDS acquisition script.[47] The number of scans was 16, the length of the $\pi/2$ hard pulse 16.25 μs, and the repetition time 3 s. The total number of acquisition steps was 66, and the total experiment time was 58 min.

https://dx.doi.org/10.1021/acs.analchem.0c01523
Anal. Chem. 2020, 92, 9948−9955

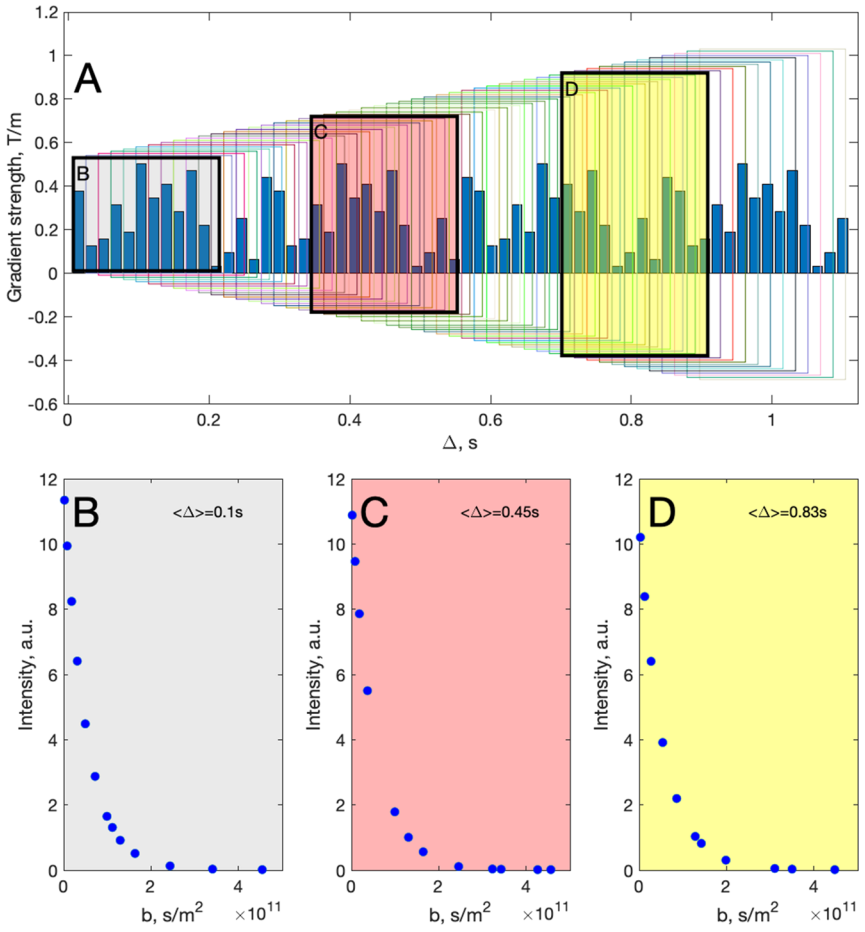

Figure 2. TR-restricted diffusion experiment. (A) Repeating random gradient strengths while the Δ value is linearly increased. The experiment is cut into overlapping frames that are used to calculate diffusion coefficients. (B–D) Examples of signal intensities at three different average times (Δ).

After the acquisition, the data were divided into overlapping frames as described in refs 39 and 40 and then the diffusion coefficient was determined by a single-exponential fit. To choose the optimal frame size, the fitting error was plotted as a function of the number of points used for calculation along with the value of the mean Δ time of the first frame. The optimal frame size (nine points) was chosen from the global minimum of the product of the two parameters mentioned above. Additionally, to confirm the proper choice of the fitting function, the diffusion coefficient distributions were calculated using the ITAMeD method.[44] These distributions revealed only a single diffusion component. Furthermore, to demonstrate the frame size effect, the same procedure was repeated for nine different frame sizes ranging from 4 to 31 points.

Restricted Diffusion. In the case of restricted diffusion, the observed apparent diffusion coefficient D is dependent on Δ. When Δ is short[3]

$$\frac{D(\Delta)}{D_0} = 1 - \frac{4}{9\sqrt{\pi}} \times \frac{S}{V} \times \sqrt{D_0\Delta} \tag{1}$$

where D_0 is the diffusion coefficient at $\Delta = 0$ and S/V is the surface:volume ratio of the porous material with smooth boundaries. Here, the S/V value of the wood sample was determined by fitting eq 1 with the D versus Δ data, when $\Delta \leq 200$ ms.

The overall Δ dependence of D can be approximated by[3]

$$\frac{D(\Delta)}{D_0} = 1 - \left(1 - \frac{1}{\alpha}\right)\frac{c\sqrt{\Delta} + \left(1 - \frac{1}{\alpha}\right)\frac{\Delta}{\theta}}{\left(1 - \frac{1}{\alpha}\right) + c\sqrt{\Delta} + \left(1 - \frac{1}{\alpha}\right)\frac{\Delta}{\theta}} \tag{2}$$

where

$$c = \frac{4}{9\sqrt{\pi}} \times \frac{S}{V} \times \sqrt{D_0} \tag{3}$$

where α is the tortuosity and θ is a pore scaling constant. The tortuosity of the wood sample was determined by fitting eq 2 with the overall D versus Δ data, using the S/V values given by the short Δ fit.

The width of the lumens inside the tracheid cells (A) along the radial direction was calculated from the S/V parameter value assuming the square-based cuboid geometry and the length of the lumen along the longitudinal direction of 2.76 mm as reported by Kekkonen et al.[5]

RESULTS AND DISCUSSION

We studied restricted diffusion of water molecules in a water-saturated thermally modified pine wood (*P. sylvestris*) sample. The axis of the cylindrical sample was along the radial direction, i.e., perpendicular to the long (2–4 mm) and narrow (10–40 μm) tracheid cells, which comprise ∼93% of the volume of pine.[48] As the magnetic field gradient was along the sample axis, the cell walls restricted significantly the diffusion

https://dx.doi.org/10.1021/acs.analchem.0c01523
Anal. Chem. 2020, 92, 9948–9955

of free water along the studied direction. The restricted diffusion phenomenon was studied with two nonconventional methods: time-resolved and ultrafast $D-T_2$. The methods are different in the basic acquisition principles, but they both accelerate the acquisition significantly and provide similar data. They have different strengths, weaknesses, and sources of errors. Therefore, they can be used as complementary tools or one of the methods can be chosen for a specific situation.

Time-Resolved Diffusion NMR. TR acquisition was performed with 66 gradient strength steps. The experiment time was equivalent to that of one conventional diffusion NMR experiment with the same number of steps. As described in previous studies of TR diffusion NMR,[39,40] the number of gradient steps to reconstruct a single frame (which corresponds to a single average Δ value) can be adjusted after the acquisition. The optimal size of the frame is determined by balancing the fitting errors originated from too few points for a good fit to extract the diffusion coefficient and too much averaging of Δ values if the frame size is too large (see Figure 3A). The effect is illustrated in Figure 3B. For

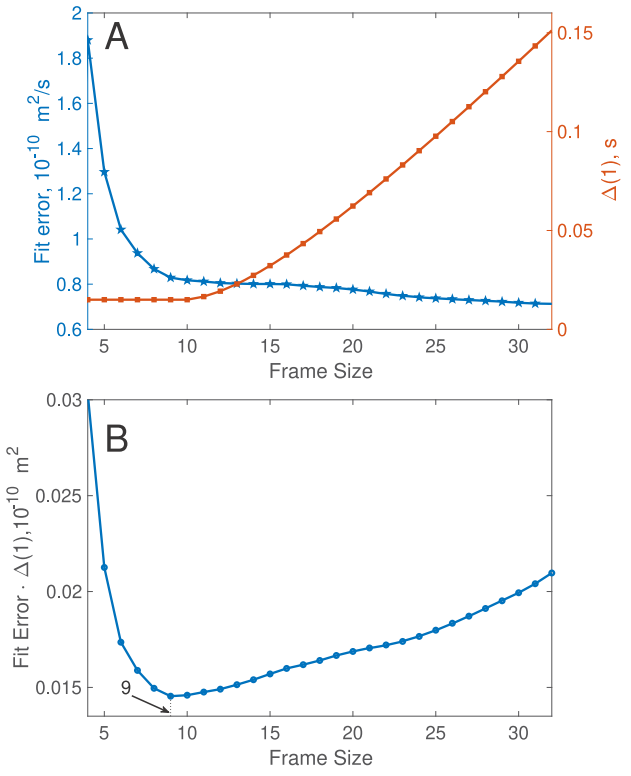

Figure 3. (A) Blue line showing the fit error (standard deviation of D obtained from the fit) and red line showing the average Δ in the first frame as a function of frame size for TR-DOSY analysis. (B) Product of the two parameters shown in panel A allowing us to determine the optimal frame size.

a small frame size, the curve is dominated by the large error. The overall error decreases with every added step. The other effect related to the frame size is the averaging of Δ. The effect is visible in Figures 3A and 4. One can easily see that too much averaging is stripping the data of any relevancy by obscuring the short time decrease of the diffusion coefficient. On the other hand, an overly small frame causes a significant fitting error. Therefore, the optimal size of the frame must be carefully chosen. A good way to estimate the optimal frame size is to analyze the product of the fitting error and the average value of Δ of the first frame (as shown in Figure 3B).

The resulting relationship between the apparent diffusion coefficient observed in the TR diffusion NMR experiment and Δ (or, to be more precise, average Δ, ⟨Δ⟩) generally follows the expected behavior (see Figure 5). For a small Δ, the D is highest as the effect of restricted diffusion is the weakest and then decreases with an increase in Δ, approaching asymptotically $\alpha^{-1}D_0$, where α is the tortuosity.

It is worth mentioning that the primary advantage of the method, i.e., the high number of points in the final plot giving an almost continuous dependence of diffusion coefficient on Δ, enables one to recognize the measurement errors much easier than in the classic approach, where one usually has only a few discrete Δ points. Therefore, it is much harder to localize the faulty data point due to some sudden disturbance in the conventional experiments.

Ultrafast $D-T_2$. The UF DOSY measurements were based on the UF $D-T_2$ pulse sequence presented in Figure 1A. The sequence allows one to sample both diffusion and transverse relaxation space but without spectral information (which for the studied sample is not relevant, as the spectrum includes only a single water peak). Due to the spatial encoding of the diffusion dimension, the whole diffusion decay curve corresponding to each Δ is measured in a single scan. However, the signal-to-noise ratio (SNR) is decreased due to spatial encoding (typically by a factor of ∼4).[29] The observed diffusion coefficients shown in Figure 5 behave similarly to TR. There are some deviations from the trend line visible in the curve due to the relatively low SNR.

The method also provides information about transverse relaxation. The $D-T_2$ correlation maps are shown in Figure 6. As expected, the T_2 values remain constant, while diffusion coefficient decreases with an increase in Δ. The T_2 resolution in the $D-T_2$ correlation maps would be highly useful for a system including two or more different kinds of pores with significantly different pore sizes. In that case, different kinds of pores should be resolved in the T_2 direction, and the restricted diffusion analysis could be performed separately for each pore type.

Comparison between the Time-Resolved and Ultrafast Methods. The apparent diffusion coefficients measured by the TR and UF methods are in relatively good agreement (see Figure 5). Both methods provide similar temporal resolution in practically identical measurement times, when the numbers of Δ steps and scans are equal. The resulting D versus Δ behavior is also in good agreement with the previous conventional diffusion NMR study of pine wood samples.[49]

The parameter values resulting from the fits of eqs 1 and 2 with the D versus Δ data are listed in Table 1. The values extracted from the UF and TR experiments are close to each other. The values of lumen size (20.0 and 21.5 μm) are in good agreement with the previously reported measurements of the same sample.[5] The values of tortuosity are high (11.0 and 12.5), which is as expected as the lumens are not well-connected in the radial direction.

Even though the methods provide comparable results, one should not forget that they are based on completely different acquisitions of the indirect direction, leading to different strengths and weaknesses. The differences are summarized below.

The UF method allows one to acquire the whole diffusion decay curve at each Δ. Thus, it provides the apparent diffusion

https://dx.doi.org/10.1021/acs.analchem.0c01523
Anal. Chem. 2020, 92, 9948−9955

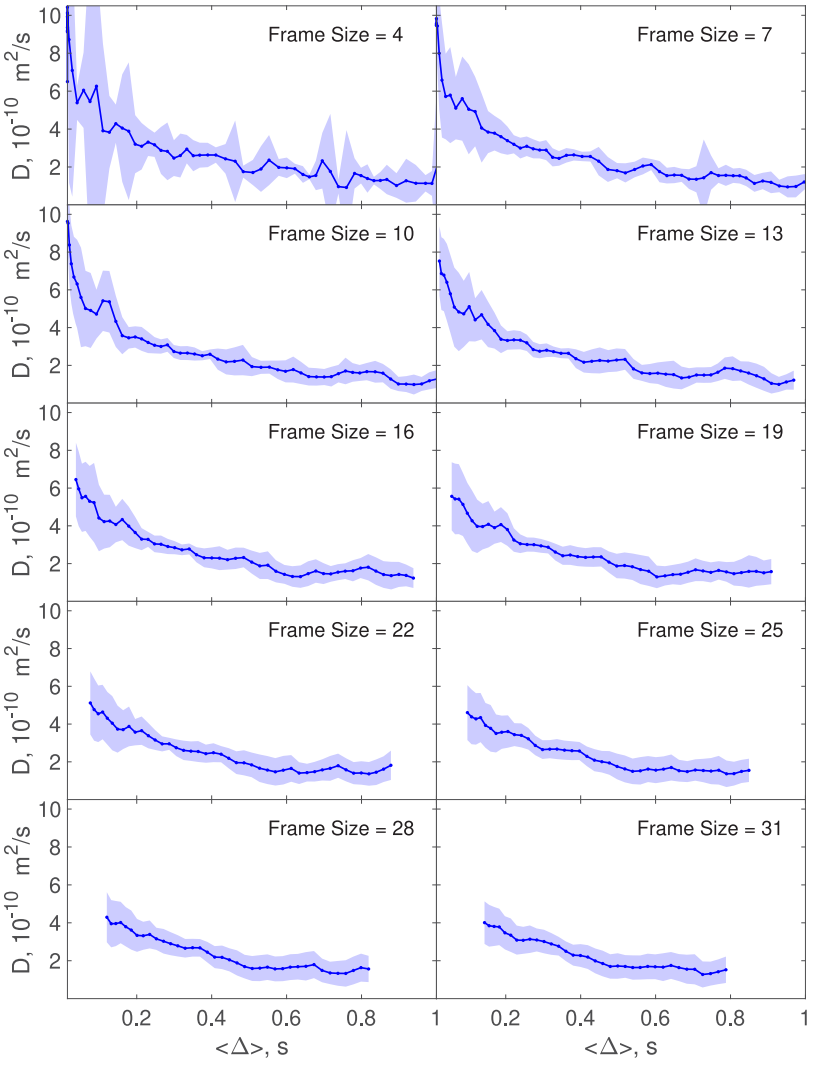

Figure 4. Effect of frame size on the restricted diffusion profile in TR.

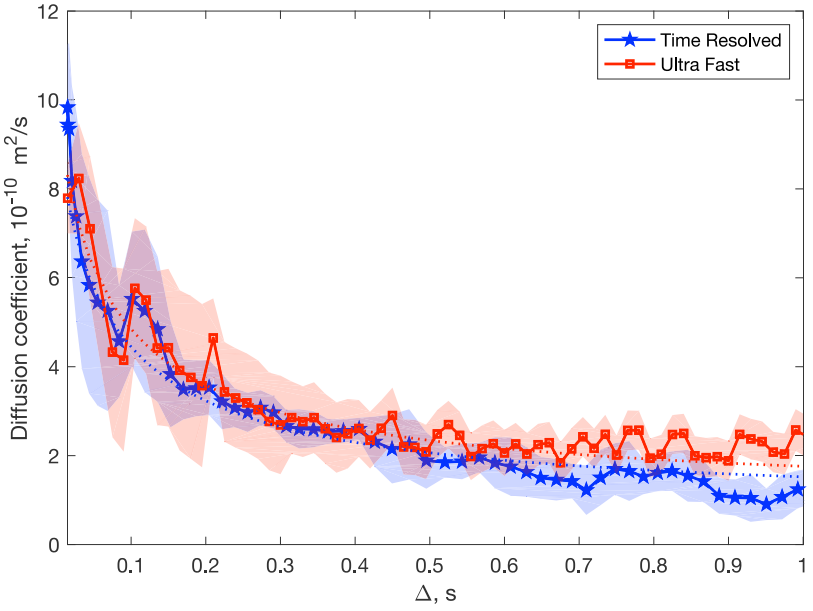

Figure 5. Apparent diffusion coefficients of free water in pine wood (in the radial direction) as a function of diffusion delay Δ measured by time-resolved and ultrafast DOSY. The color bands represent the fitting errors. Dotted lines show the fits of eq 2 with the data.

https://dx.doi.org/10.1021/acs.analchem.0c01523
Anal. Chem. 2020, 92, 9948−9955

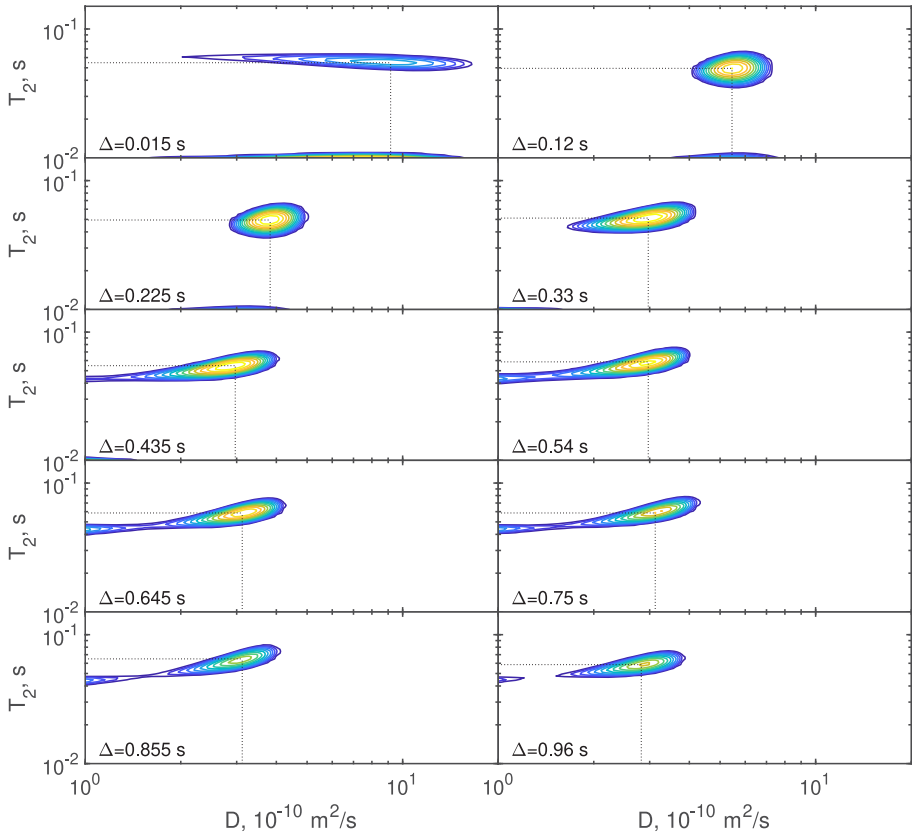

Figure 6. Ultrafast $D-T_2$ maps.

Table 1. Surface:Volume Ratios (S/V), Lumen Sizes (A), Bulk Diffusion Coefficients (D_0), Tortuosities (α), and Pore Size Scaling Constants (θ) of Thermally Modified Pine in the Radial Direction Measured by UF and TR Methods

experiment	S/V (m^{-1})	A (μm)	D_0 ($\times 10^{-10}$ m^2/s)	α	θ
TR	200000 ± 3000	20.0 ± 0.3	10.40 ± 0.07	12.5 ± 1.1	0.090 ± 0.004
UF	186000 ± 3000	21.5 ± 0.3	11.03 ± 0.09	11.02 ± 1.2	0.096 ± 0.008

coefficients at exact values of Δ. On the other hand, the TR method measures an average diffusion coefficient corresponding to the average Δ of the frame (⟨Δ⟩), because the points of the indirect dimension are sampled with incremented Δ. Consequently, the UF method provides complete and exact measurement data, while the TR method results in averaged and undersampled data.

The spatial encoding decreases the sensitivity of the UF method (typically by a factor of ∼4),[29] because the sample is virtually split into layers. Therefore, the TR method results in a higher SNR per scan than the UF method, and for samples with a relatively low SNR, it may be advisible to use the TR method instead UF. However, the sample studied herein had a high water concentration, and therefore, the sensitivity difference did not influence the results. Additionally, the spatial encoding profile is highly affected by the coil sensitivity profile and the inhomogeneity of the sample, and these factors must be eliminated by the experimentally measured sample and excitation−detection profile (as was done in this work). The wood sample used in the experiment is a good example of such a problem. In Figure 7, it is clearly visible that annual rings are strongly influencing the spatial encoding and the signal correction is required. On the other had, this work demonstrates nicely that the spatial encoding works well also

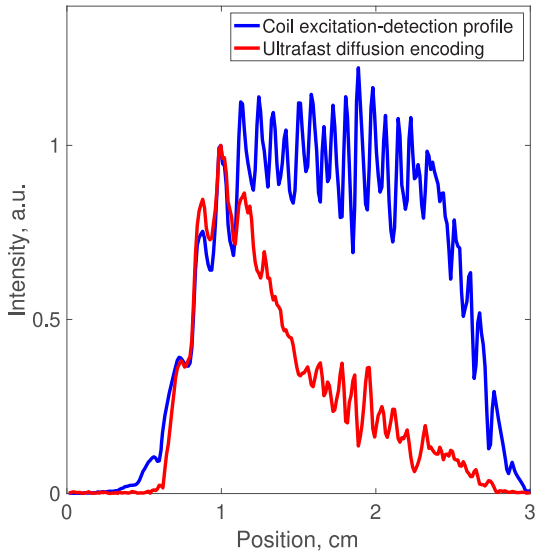

Figure 7. Effect of the inhomogeneity of the sample on the spatial encoding profile. The blue line is the coil sensitivity profile, and the red line is the diffusion decay profile. The signal oscillations are due to the annual rings of the wood.

https://dx.doi.org/10.1021/acs.analchem.0c01523
Anal. Chem. 2020, 92, 9948−9955

with inhomogeneous samples when the profile correction is performed.

The NMR parameter corresponding to the direct dimension was the frequency in the TR experiments, while it was T_2 in the UF experiments. In this study, both the frequency and T_2 spectra included only one peak (the component of bound water with a short T_2 was effectively filtered out in the diffusion encoding), which did not provide any additional information about the wood sample. However, in some cases, such as analysis of complex mixtures of fluids, the frequency resolution may be highly desirable, while some other systems, such as porous materials with significantly different pore sizes, may benefit from T_2 resolution. On the other hand, the TR can be easily modified in a $D-T_2$ type experiment using a CPMG block in the detection. Furthermore, spectral information can be added to the UF-DOSY experiment with echo planar spectroscopic imaging (EPSI) type detection.[23−25]

An important practical issue is the laboriousness of the experiment setting. While the TR method has already been automated[47] and acquisition scripts can be easily adjusted for a particular case of TR, the UF $D-T_2$ experiment has not yet been automated and therefore required manual calibration of the chirp pulse phase and power, as well as the gradient strength, ideally, for each Δ value. However, in this project, after 100 ms, these parameters were changed only every 100 ms of Δ, reducing significantly the required number of calibrations (from 67 to 15). On the other hand, with programming, it is possible to automate the UF measurement process similarly to the TR.

Experimental errors will also be manifested in different ways in the TR and UF data. The effect of a single wrong point in the TR signal amplitude data will be decreased by surrounding points due to inside frame averaging, but it will affect many frames over a broad region of average Δ times. On the other hand, there is no such averaging effect in the UF method, and an artificial D data point can be easily spotted as it is usually a single point that stands out from the general trend (see the data point in Figure 5 at ∼210 ms).

After the thorough discussion about differences between the two methods, we conclude that, if the signal is strong enough and the sample is uniform enough (and if we do not consider the time for setting the experimental parameters), the UF method provides more complete and accurate data than TR with the same experiment time and temporal resolution, as full diffusion decay curves are collected at each Δ value, and there is no such Δ averaging effect as in the TR. On the other hand, if a higher SNR and an easier setup of the experiment are desired, TR may be the method of choice.

CONCLUSIONS

In this work, we demonstrate the adaptation of time-resolved and ultrafast diffusometry experiments for restricted diffusion analysis. We show that both methods provide significant (1−2 orders of magnitude) acceleration of the measurements, allowing us to gather many more data points in a given time and therefore providing a more detailed description of the restricted diffusion phenomena. The UF method gives more complete and accurate data, but the TR method provides a higher SNR, easier setting of experimental parameters, and a better tolerance for sample inhomogeneity. Both methods resulted in reasonable values of lumen size and tortuosity of the thermally modified pine wood samples. The data of the direct dimension (frequency or T_2) were not exploited in this study, but it could prove to be highly useful in the analysis of more complex samples such as mixtures of fluids or porous materials with highly heterogeneous pore structures. Furthermore, the acceleration of the restricted diffusion experiments could allow one to add additional frequency or relaxation time dimensions to gain more information about complex systems.

AUTHOR INFORMATION

Corresponding Author

Ville-Veikko Telkki − *NMR Research Unit, University of Oulu, 90014 Oulu, Finland;* orcid.org/0000-0003-0846-6852; Email: ville-veikko.telkki@oulu.fi

Authors

Mateusz Urbańczyk − *NMR Research Unit, University of Oulu, 90014 Oulu, Finland;* orcid.org/0000-0001-6085-1593

Yashu Kharbanda − *NMR Research Unit, University of Oulu, 90014 Oulu, Finland;* orcid.org/0000-0002-1082-0139

Otto Mankinen − *NMR Research Unit, University of Oulu, 90014 Oulu, Finland; Oulu Functional NeuroImaging Group, Research Unit of Medical Imaging, Physics and Technology, Medical Research Center Oulu, University of Oulu and Oulu University Hospital, 90029 Oulu, Finland;* orcid.org/0000-0002-0580-090X

Complete contact information is available at: https://pubs.acs.org/10.1021/acs.analchem.0c01523

Notes

The authors declare no competing financial interest.

ACKNOWLEDGMENTS

The authors acknowledge the financial support of the European Research Council (ERC) under Horizon 2020 (H2020/2018-2022/ERC Grant Agreement 772110), the Academy of Finland (Grants 289649, 294027, and 319216), the Kvantum institute (University of Oulu), the CA15209 COST Action (EURELAX), the Finnish Cultural Foundation (Fanny and Yrjö Similä fund), the Fortum Foundation, and The University of Oulu Scholarship Foundation (Science Fund).

REFERENCES

(1) Valiullin, R. *Diffusion NMR of Confined Systems: Fluid Transport in Porous Solids and Heterogeneous Materials*; Royal Society of Chemistry, 2017; p 576.

(2) Mitra, P. P.; Sen, P. N. *Phys. Rev. B: Condens. Matter Mater. Phys.* **1992**, *45*, 143−156.

(3) Latour, L. L.; Mitra, P. P.; Kleinberg, R. L.; Sotak, C. H. *J. Magn. Reson., Ser. A* **1993**, *101*, 342−346.

(4) Kekkonen, P. M.; Ylisassi, A.; Telkki, V.-V. *J. Phys. Chem. C* **2014**, *118*, 2146−2153.

(5) Kekkonen, P. M.; Telkki, V.-V.; Jokisaari, J. *J. Phys. Chem. C* **2010**, *114*, 18693−18697.

(6) Satterfield, C. N.; Colton, C. K.; Pitcher, W. H. *AIChE J.* **1973**, *19*, 628−635.

(7) Javed, M. A.; Ahola, S.; Håkansson, P.; Mankinen, O.; Aslam, M. K.; Filippov, A.; Shah, F. U.; Glavatskih, S.; Antzutkin, O. N.; Telkki, V.-V. *Chem. Commun.* **2017**, *53*, 11056−11059.

(8) Anisimov, A. V.; Sorokina, N. Y.; Dautova, N. R. *Magn. Reson. Imaging* **1998**, *16*, 565−568.

(9) Helmer, K. G.; Dardzinski, B. J.; Sotak, C. H. *NMR Biomed.* **1995**, *8*, 297−306.

https://dx.doi.org/10.1021/acs.analchem.0c01523
Anal. Chem. 2020, 92, 9948−9955

(10) Veith, S. R.; Hughes, E.; Pratsinis, S. E. *J. Controlled Release* **2004**, *99*, 315−327.
(11) Lin, G.; Zheng, S.; Liao, X. *J. Magn. Reson.* **2016**, *272*, 25−36.
(12) Kharbanda, Y.; Urbańczyk, M.; Laitinen, O.; Kling, K.; Pallaspuro, S.; Komulainen, S.; Liimatainen, H.; Telkki, V.-V. *J. Phys. Chem. C* **2019**, *123*, 30986−30995.
(13) Hwang, S.; Kärger, J. *NMR diffusometry with guest molecules in nanoporous materials*; 2019.
(14) Splith, T.; Fröhlich, D.; Henninger, S. K.; Stallmach, F. *J. Magn. Reson.* **2018**, *291*, 40−46.
(15) Frydman, L.; Scherf, T.; Lupulescu, A. *Proc. Natl. Acad. Sci. U. S. A.* **2002**, *99*, 15858−15862.
(16) Pelupessy, P. *J. Am. Chem. Soc.* **2003**, *125*, 12345−12350.
(17) Tal, A.; Frydman, L. *Prog. Nucl. Magn. Reson. Spectrosc.* **2010**, *57*, 241−292.
(18) Frydman, L.; Blazina, D. *Nat. Phys.* **2007**, *3*, 415−419.
(19) Telkki, V.-V. *Magn. Reson. Chem.* **2018**, *56*, 619−632.
(20) Telkki, V.-V.; Zhivonitko, V. V. *Annu. Rep. NMR Spectrosc.* **2019**, *97*, 83−119.
(21) Callaghan, P. T. *Translational Dynamics and Magnetic Resonance: Principles of Pulsed Gradient Spin Echo NMR*; Oxford University Press, 2011.
(22) Thrippleton, M. J.; Loening, N. M.; Keeler, J. *Magn. Reson. Chem.* **2003**, *41*, 441−447.
(23) Shrot, Y.; Frydman, L. *J. Magn. Reson.* **2008**, *195*, 226−231.
(24) Guduff, L.; Kuprov, I.; Van Heijenoort, C.; Dumez, J. N. *Chem. Commun.* **2017**, *53*, 701−704.
(25) Hamdoun, G.; Guduff, L.; Van Heijenoort, C.; Bour, C.; Gandon, V.; Dumez, J. N. *Analyst* **2018**, *143*, 3458−3464.
(26) Ahola, S.; Telkki, V.-V. *ChemPhysChem* **2014**, *15*, 1687−1692.
(27) King, J. N.; Lee, V. J.; Ahola, S.; Telkki, V.-V.; Meldrum, T. *Angew. Chem., Int. Ed.* **2016**, *55*, 5040−5043.
(28) King, J. N.; Fallorina, A.; Yu, J.; Zhang, G.; Telkki, V.-V.; Hilty, C.; Meldrum, T. *Chemical Science* **2018**, *9*, 6143−6149.
(29) Ahola, S.; Zhivonitko, V. V.; Mankinen, O.; Zhang, G.; Kantola, A. M.; Chen, H. Y.; Hilty, C.; Koptyug, I. V.; Telkki, V.-V. *Nat. Commun.* **2015**, *6*, 8363.
(30) Mankinen, O.; Hollenbach, J.; Ahola, S.; Matysik, J.; Telkki, V.-V. *Micropor. Mesopor. Mater.* **2018**, *269*, 75−78.
(31) Mankinen, O.; Zhivonitko, V. V.; Selent, A.; Mailhiot, S.; Komulainen, S.; Prisle, N. L.; Ahola, S.; Telkki, V.-V. *Nat. Commun.* **2020**, *11*, 3251.
(32) Mayzel, M.; Rosenlöw, J.; Isaksson, L.; Orekhov, V. Y. *J. Biomol. NMR* **2014**, *58*, 129−39.
(33) Shchukina, A.; Urbańczyk, M.; Kasprzak, P.; Kazimierczuk, K. *Concepts Magn. Reson., Part A* **2017**, *46A*, e21429.
(34) Dass, R.; Kozminski, W.; Kazimierczuk, K. *Anal. Chem.* **2015**, *87*, 1337−1343.
(35) Gołowicz, D.; Kazimierczuk, K.; Urbańczyk, M.; Ratajczyk, T. *ChemistryOpen* **2019**, *8*, 196−200.
(36) Gołowicz, D.; Kasprzak, P.; Orekhov, V.; Kazimierczuk, K. *Prog. Nucl. Magn. Reson. Spectrosc.* **2020**, *116*, 40−55.
(37) Bermel, W.; Dass, R.; Neidig, K.-P.; Kazimierczuk, K. *Chem. - Eur. J.* **2014**, *15*, 2217−2220.
(38) Gołowicz, D.; Urbańczyk, M.; Shchukina, A.; Kazimierczuk, K. *J. Magn. Reson.* **2018**, *294*, 1−6.
(39) Urbańczyk, M.; Bernin, D.; Czuroń, A.; Kazimierczuk, K. *Analyst* **2016**, *141*, 1745−1752.
(40) MacDonald, T. S.; Price, W. S.; Beves, J. E. *ChemPhysChem* **2019**, *20*, 926−930.
(41) Oikonomou, M.; Asencio-Hernández, J.; Velders, A. H.; Delsuc, M.-A. *J. Magn. Reson.* **2015**, *258*, 12−16.
(42) *ThermoWood Handbook*; Finnish Thermowood Association and International ThermoWood Association: Helsinki, 2003.
(43) Stejskal, E. O.; Tanner, J. E. *J. Chem. Phys.* **1965**, *42*, 288.
(44) Urbańczyk, M.; Bernin, D.; Koźmiński, W.; Kazimierczuk, K. *Anal. Chem.* **2013**, *85*, 1828−1833.
(45) Urbańczyk, M.; Koźmiński, W.; Kazimierczuk, K. *Angew. Chem., Int. Ed.* **2014**, *53*, 6464−6467.
(46) Urbańczyk, M.; Nowakowski, M.; Koźmiński, W.; Kazimierczuk, K. *J. Biomol. NMR* **2017**, *68*, 155−161.
(47) Urbańczyk, M.; Shchukina, A.; Gołowicz, D.; Kazimierczuk, K. *Magn. Reson. Chem.* **2019**, *57*, 4−12.
(48) Kettunen, P. O. *Wood Structure and Properties*; Trans Tech Publications, 2006.
(49) Wycoff, W.; Pickup, S.; Cutter, B.; Miller, W.; Wong, T. C. *Wood Fiber Sci.* **2000**, *32*, 72−80.

https://dx.doi.org/10.1021/acs.analchem.0c01523
Anal. Chem. 2020, 92, 9948−9955